Superconductivity, Charge Density Wave, and Supersolidity in Flat Bands with a Tunable Quantum Metric

Johannes S. Hofmann, Erez Berg, and Debanjan Chowdhury

Phys. Rev. Lett. **130**, 226001 — Published 31 May 2023

DOI: 10.1103/PhysRevLett.130.226001

Superconductivity, charge density wave, and supersolidity in flat bands with tunable quantum metric

Johannes S. Hofmann,[1] Erez Berg,[1,*] and Debanjan Chowdhury[2,†]

[1] *Department of Condensed Matter Physics, Weizmann Institute of Science, Rehovot, 76100, Israel.*
[2] *Department of Physics, Cornell University, Ithaca, New York 14853, USA.*

Predicting the fate of an interacting system in the limit where the electronic bandwidth is quenched is often highly non-trivial. The complex interplay between interactions and quantum fluctuations driven by the band geometry can drive competition between various ground states, such as charge density wave order and superconductivity. In this work, we study an electronic model of topologically-trivial flat bands with a continuously tunable Fubini-Study metric in the presence of on-site attraction and nearest-neighbor repulsion, using numerically exact quantum Monte Carlo simulations. By varying the electron filling and the minimal spatial extent of the localized flat-band Wannier wavefunctions, we obtain a number of intertwined orders. These include a phase with coexisting charge density wave (CDW) order and superconductivity, i.e., a supersolid. In spite of the non-perturbative nature of the problem, we identify an analytically tractable limit associated with a 'small' spatial extent of the Wannier functions and derive a low-energy effective Hamiltonian that can well describe our numerical results. We also provide unambiguous evidence for the violation of any putative *lower* bound on the zero-temperature superfluid stiffness in geometrically non-trivial flat bands.

Introduction.- Superconductivity in narrow-band systems has attracted enormous attention, triggered in part by the discovery of two-dimensional moiré materials [1] and the fundamental theoretical aspects that remain poorly understood [2]. The limit of flat bands is particularly interesting as a possible route to optimize the superconducting T_c (in the presence of an effective attraction), because of the diverging density of states. In this situation, it has been predicted that T_c is proportional to $|U|$, the strength of the effective attractive interaction [3–5]. However, the lack of electronic dispersion also implies a reduced superconducting phase stiffness, limiting T_c. Moreover, a plethora of competing non-superconducting phases may arise.

Topological flat bands, that do not admit an exponentially localized basis in real space [6], have been proposed to generate a non-zero phase stiffness within Bardeen-Cooper-Schrieffer (BCS) mean-field theory [7]. Numerically exact determinant quantum Monte Carlo (DQMC) [8] calculations have indeed provided an unambiguous and non-perturbative demonstration for $T_c \propto |U|$ [9–12] for topological flat-bands, where $|U|$ denotes the strength of an on-site attraction. Even for this simplified problem, the normal state for temperature $T > T_c$ exhibits strong nearly degenerate density and pairing fluctuations due to an emergent SU(2) symmetry [13], such that the ground state is highly susceptible to competing orders. Within BCS mean-field theory and for models satisfying a set of restrictive conditions, lower bounds on the zero-temperature phase stiffness have been proposed [7, 14–16], and shown to be governed by the integrated Fubini-Study metric (up to an energy-scale set by the superconducting gap). Beyond mean-field theory, upper bounds on the stiffness have also been proven [17–19].

This naturally leads to the following questions when departing from the BCS paradigm: (i) What is the nature of the competing phases and associated quantum phase transitions that arise in flat bands as a function of various microscopic tuning parameters? (ii) How does varying the minimal spatial extent of the localized Wannier functions tune the system between different orders? (iii) Is there a theoretical limit in which this band competition can be explored in a controlled fashion without resorting to uncontrolled mean-field theory? (iv) Can infinitesimal perturbations drive competing instabilities leading to substantial violations of proposed lower bounds on T_c?

In this Letter, we study a concrete electronic Hamiltonian for topologically trivial flat bands, where the minimal spatial extent of the exponentially localizable Wannier functions can be tuned *continuously* without affecting the band dispersion. Using unbiased DQMC simulations, we will demonstrate that such a model supports superconductivity with a wide fluctuation regime and obtain the detailed dependence of T_c on the spatial extent of the Wannier functions. Additionally, by varying the strength of further-neighbor interactions, the electronic density, and the spatial extent of the Wannier functions, we can drive continuous phase transitions to charge density wave (CDW) and supersolid phases within the same flat-band limit. Remarkably, we can use the spatial extent of the Wannier functions as a 'small' parameter to derive an effective pseudospin Hamiltonian that helps explain the intertwined superconductivity, CDW, and supersolid orders in this flat-band model. Finally, the ability to tune continuously between various (non-) superconducting phases allows us to violate any putative lower bound on T_c.

Model.- We define a two-orbital, spinful electronic model with local interactions. The model, first intro-

* erez.berg@weizmann.ac.il
† debanjanchowdhury@cornell.edu

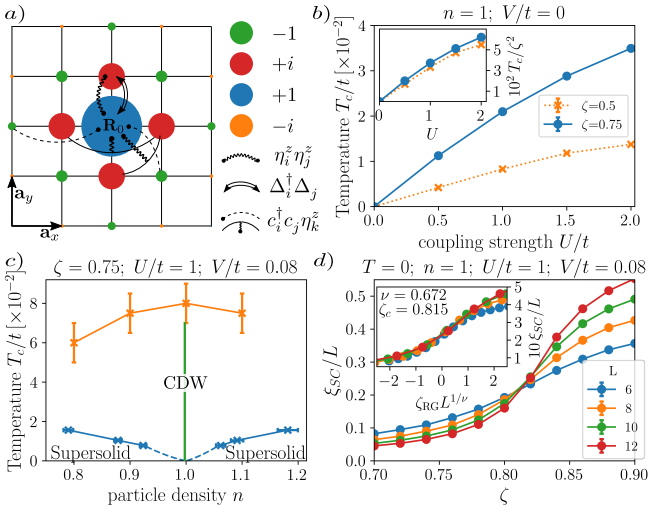

FIG. 1. a) The localized Wannier function, $\Phi_{\mathbf{R}_0}(\mathbf{r})$. The area (color) of the disc is proportional to the amplitude (phase). b) The superconducting T_c increases with $\zeta^2|U|$ (see also inset). c) The phase diagram for $V = 0.08$. At $n = 1$, the system is an insulating CDW for $T \lesssim 0.075$, and when doped, the excess carriers lead to a supersolid. d) The normalized superconducting correlation length ξ_{SC}/L at $T = 0$ across a CDW to supersolid transition with increasing ζ, consistent with a $(2+1)-$dimensional XY phase transition ($\zeta_c = 0.815$, $\zeta_{RG} = (\zeta - \zeta_c)/\zeta_c$) for different system sizes, L .

duced in Ref. [20], is time-reversal symmetric, and resides on a square two-dimensional lattice with two orbitals per site. We will focus on densities in the vicinity of one electron per unit cell, corresponding to quarter filling. The model exhibits two pairs of perfectly flat bands at energies, $\varepsilon_{\mathbf{k}} = \pm t$, where t sets the overall scale associated with the microscopic hopping parameters. The energy gap is $\Delta_{\rm gap} = 2t$.

The non-interacting part of the Hamiltonian reads

$$\begin{aligned} H_0 &= -t\sum_{\mathbf{k}} \hat{\mathbf{c}}^\dagger_{\mathbf{k}} \left(\lambda_x \sin\alpha_{\mathbf{k}} + \sigma_z\lambda_y \cos\alpha_{\mathbf{k}} + \mu\lambda_0\right)\hat{\mathbf{c}}_{\mathbf{k}}, \\ \alpha_{\mathbf{k}} &= \zeta(\cos k_x a + \cos k_y a). \end{aligned} \tag{1}$$

Here, $\hat{\mathbf{c}}^\dagger_{\mathbf{k}}$ is a vector of operators $\hat{c}^\dagger_{\mathbf{k},l,s}$ which create electrons with momentum $\mathbf{k}$ and spin $s =\uparrow,\downarrow$ in orbital $l = 1, 2$. The Pauli-matrices $\sigma_{j=0,x,y,z}$ and $\lambda_{j=0,x,y,z}$ act on the spin and orbital indices, respectively, and $a = |\mathbf{a}_x|$ is the length of the primitive lattice vectors. Regardless of t, the dimensionless parameter ζ controls the spatial extent of the localized Wannier functions, $\Phi_{\mathbf{R}_0}(\mathbf{r}) \sim (i\zeta)^{|\delta_x|+|\delta_y|} + \mathcal{O}(\zeta^{|\delta_x|+|\delta_y|+2})$, where $\boldsymbol{\delta} = (\mathbf{r} - \mathbf{R}_0)/a$; see Fig. 1(a). The quantum geometric tensor, $\mathcal{G}_{ij}$, is simple—the imaginary part (i.e. Berry curvature) vanishes everywhere in the BZ while the real part (i.e. the Fubini-Study metric) is finite and integrates to $\zeta^2 a^2/2$ [21]. Note that the metric depends on how the orbitals are embedded in real space; here, both orbitals are located at the center of the unit cell in the $x-y$ plane, respecting C_4 rotation symmetry [22].

At a fractional filling of the lower band ($\varepsilon_{\mathbf{k}} = -t$), we will study the effect of on-site attraction, $U > 0$, and nearest-neighbor interaction, V,

$$H_{\rm int} = -\frac{U}{2}\sum_{\mathbf{r},l}\delta\hat{n}^2_{\mathbf{r},l} + V\sum_{\langle\mathbf{r},\mathbf{r}'\rangle,l}\delta\hat{n}_{\mathbf{r},l}\,\delta\hat{n}_{\mathbf{r}',l}\,, \tag{2}$$

where $\delta\hat{n}_{\mathbf{r},l} = \sum_s \hat{c}^\dagger_{\mathbf{r},l,s}\hat{c}_{\mathbf{r},l,s} - 1$ refers to the (shifted) density operator in orbital l at site $\mathbf{r}$. The above model, $H = H_0 + H_{\rm int}$, is free of the infamous sign problem as long as $U \geq 4|V|$. Before analyzing the model numerically, we derive the effective Hamiltonian that illustrates the competition between various ordering tendencies. This analytical approach relies on a controlled expansion for small ζ, but agrees qualitatively with the non-perturbative results obtained using DQMC.

Analytical results for small ζ.– We focus on the limit of $\zeta \ll 1$ and $T, V \ll U \ll \Delta_{\rm gap}(= 2t)$, that allows us to project the interaction to the lower "active" band. The localized Wannier wave function of the lower band, centered around $\mathbf{r} = \mathbf{R}_0$, $\Phi_{\mathbf{R}_0,s}(\mathbf{r}) = \frac{1}{\sqrt{2}L^2}\sum_{\mathbf{k}} e^{i\mathbf{k}(\mathbf{R}_0-\mathbf{r})}e^{is\lambda_z\alpha_{\mathbf{k}}/2}(1,-si)^\dagger$ [21], is depicted in Fig. 1(a). Upon introducing new operators, $\hat{c}^\dagger_{\mathbf{r},l,s} \mapsto \sum_{\mathbf{r}'}\Phi^*_{\mathbf{r},s}(\mathbf{r}',l)\hat{d}^\dagger_{\mathbf{r}',s}$, the projected interaction Hamiltonian in the $\zeta \ll 1$ limit takes the form of an effective XXZ model supplemented by other terms,

$$\begin{aligned} \widetilde{H_{\rm int}} &= -\frac{U_{\rm eff}}{2}\sum_{\mathbf{r}}(2\hat{\eta}^z_{\mathbf{r}})^2 + \frac{U\zeta^2}{32}\sum_{\mathbf{r}}\hat{\eta}^z_{\mathbf{r}}(2\hat{B}^\delta_{\mathbf{r}} - \hat{B}^{2\delta}_{\mathbf{r}}) \\ &\quad - \sum_{\langle\mathbf{r},\mathbf{r}'\rangle}\left[J_\perp(\hat{\eta}^x_{\mathbf{r}}\hat{\eta}^x_{\mathbf{r}'} + \hat{\eta}^y_{\mathbf{r}}\hat{\eta}^y_{\mathbf{r}'}) + J_z\hat{\eta}^z_{\mathbf{r}}\hat{\eta}^z_{\mathbf{r}'}\right], \end{aligned} \tag{3}$$

with pseudospin operators, $\hat{\eta}^{j=0,x,y,z}_{\mathbf{r}} \equiv (\Psi^\dagger_{\mathbf{r}}\eta^j\Psi_{\mathbf{r}})/2$, where $\Psi^\dagger_{\mathbf{r}} = (\hat{d}^\dagger_{\mathbf{r},\uparrow}, \hat{d}_{\mathbf{r},\downarrow})$ and η^j are Pauli matrices.

The parameters, $U_{\rm eff} = U(2-\zeta^2)/4$, $J_\perp = \zeta^2 U/4$, and $J_z = \zeta^2 U/4 - 2V$. For $\zeta = 0$, the sites decouple completely and $\Phi_{\mathbf{r},s}(\mathbf{r}') \propto \delta_{\mathbf{r}\mathbf{r}'}$; only the first term in Eq. (3) survives and the ground state manifold is highly degenerate, consisting of local Cooper pairs without long-ranged phase coherence. The projected Hamiltonian also contains interaction-mediated nearest-neighbor, $\hat{B}^\delta_{\mathbf{r}} = \sum_{s,\substack{\mathbf{e}_1,\mathbf{e}_2\\ \mathbf{e}_1\neq\mathbf{e}_2}}\hat{d}^\dagger_{\mathbf{r}+\mathbf{e}_1,s}\hat{d}_{\mathbf{r}+\mathbf{e}_2,s}$, and second nearest-neighbor, $\hat{B}^{2\delta}_{\mathbf{r}} = \sum_{s,\mathbf{e}_1,\mathbf{e}_2,\,\mathbf{e}_1\neq-\mathbf{e}_2}(\hat{d}^\dagger_{\mathbf{r}+\mathbf{e}_1+\mathbf{e}_2,s}\hat{d}_{\mathbf{r},s} +$ h.c.), hopping terms, with $\mathbf{e}_{1,2} \in \{\pm\mathbf{a}_x, \pm\mathbf{a}_y\}$. In Fig. 1(a), we represent the pair hopping ($J_\perp$) and nearest-neighbor density (J_z) interactions by double-solid and wiggly lines, respectively. The interaction-mediated hoppings $\hat{B}^\delta$ and $\hat{B}^{2\delta}$ are depicted as solid and dashed lines, respectively. The interaction-mediated hopping between nearest-neighbor sites at order ζ vanishes due to chiral symmetry [21].

At finite ζ and $V = 0$, $\widetilde{H_{\rm int}}$ exhibits an emergent SU(2) symmetry [13] and strong fluctuations in the degenerate density and pairing response, without any long-range order at finite temperature. This symmetry is broken by

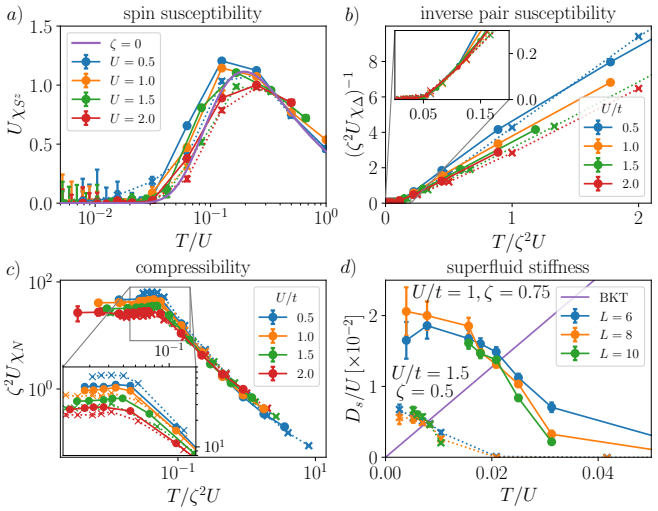

FIG. 2. (a) Spin susceptibility, $\chi_{S^z}(T)$, for different U at fixed $\zeta = 0.75$ (solid) and $\zeta = 0.5$ (dashed). The purple line, $\zeta = 0$, represents the atomic limit with a spin gap of $\Delta_{S^z} = U/4$. (b) Inverse pair susceptibility, $\chi_\Delta^{-1}(T)$, and (c) compressibility, $\chi_N(T)$, as a function of temperature obtained for same values of U as in (a). (d) Exemplary data for superfluid stiffness, $D_s(T)$, used to extract the critical temperature, T_c. Results obtained for $V = 0$.

higher-order terms in $U/\Delta_{\rm gap}$, leading to an anisotropy $\Delta J = J_\perp - J_z$ and a finite superconducting transition temperature with $T_c \propto \pi J_\perp / \log(\pi J_\perp/\Delta J)$, as shown in Fig. 1(b). The anisotropy can also be tuned by turning on V; the ground state is susceptible towards formation of an ordered CDW at a commensurate filling when $-|J_\perp| > J_z$ (Fig. 1c). Doping away from the commensurate CDW at $n = 1$ induces a density-mediated hopping and leads to a supersolid phase with long-range superconducting phase coherence (Fig. 1c). Furthermore, at $n = 1$, increasing ζ also induces a continuous transition to a supersolid ground state, consistent with the $(2+1)$-dimensional XY universality class (Fig. 1d-inset).

Numerical results.- We note that H_0 contains hopping matrix elements which decay in real-space as $t_{\boldsymbol{\delta}} \sim \zeta^{|\delta_x|+|\delta_y|}$. We truncate the range of hopping in our implementation of the DQMC computations using ALF [23, 24], neglecting terms with $|\delta_x| + |\delta_y| > 3$, leading to non-zero bandwidth $W \sim O(\zeta^4)$.

We first focus on the case of on-site interaction only ($V = 0$) at quarter filling ($n = 1$). We are interested in two-particle susceptibilities of local operators, $\hat{O}$, i.e. $\chi_O = L^{-2}\int_0^\beta d\tau \langle \hat{O}(\tau)\hat{O}(\tau = 0)\rangle$ with inverse temperature $\beta = (k_B T)^{-1}$ and imaginary time τ. For instance, for $\hat{O} \equiv S_z$, χ_{S^z} is the spin susceptibility. The results for χ_{S^z} vs. temperature are shown in Fig. 2(a) for few different interaction strengths and $\zeta = 0.5$ (dashed line) or $\zeta = 0.75$ (solid line). The data obey nearly perfect scaling of the form $\chi = f(T/U)/U$. χ_{S^z} is peaked near $T \sim 0.2U$ and shows a dramatic suppression for $T \lesssim 0.1U$. The onset of such a "pseudogap" behavior is already present in the $\zeta \to 0$ limit (purple curve in Fig. 2a), where the gap $\Delta_{S^z} = U/4$.

In addition, we examine the pairing-susceptibility, χ_Δ for $\hat{O} \equiv \Delta_s = \sum_{\mathbf{r},l}(c_{\mathbf{r},l,\uparrow}c_{\mathbf{r},l,\downarrow} + \text{h.c.})$, and the charge-compressibility, χ_N for $\hat{O} \equiv N = \sum_{\mathbf{r},l,s}(c^\dagger_{\mathbf{r},l,s}c_{\mathbf{r},l,s} - n)$. The pairing and charge fluctuations are strongly enhanced with decreasing temperature, signaling a near degeneracy between the competing tendencies towards superconductivity and phase-separation [13]; see Fig. 2(b)-(c). However, upon approaching the superconducting T_c from above, the pair-susceptibility diverges (i.e., $\chi_\Delta^{-1} \to 0$), while the compressibility saturates to a finite value.

In two dimensions, the superconducting T_c can be obtained using the criterion $D_s(T \to T_c^-) = 2T_c/\pi$ [25], where $D_s(T) = -[K_x + \Lambda_{xx}(\mathbf{q} \to 0)]/4$ is the superfluid stiffness; $\Lambda_{xx}(\mathbf{q})$ is the paramagnetic current-current correlation function at zero Matsubara frequency, and K_x is the diamagnetic current correlator [26]. In Fig. 2(d), we show the data for $D_s(T)$ for $(U, \zeta) = (1.0, 0.75)$ (solid) and $(U, \zeta) = (1.5, 0.5)$ (dashed). To a reasonable approximation, $T_c \propto U\zeta^2$, as shown in Fig. 1(b). This is expected based on our discussion of the effective XXZ model in the small ζ limit. A superconducting instability with $T_c \propto U$ has been reported in earlier DQMC computations involving topological flat-bands [9, 10], and more recently in topologically *trivial* flat-bands [12]. Our numerically exact analysis of this non-perturbative regime and the complementary analytical results obtained using the XXZ pseudospin Hamiltonian offer new insights into the role of a tunable metric in flat-band superconductors.

We now include a repulsive nearest-neighbor density interaction, $V = 0.08$, and analyze the phase diagram for a range of fillings near $n = 1$ (Fig. 1c). The main effect of the repulsive interaction is to spontaneously break the discrete translational symmetry and induce a CDW order at an ordering wavevector of (π, π). We have extracted the CDW correlation length [21, 27], $\xi_{\rm CDW}$, and the associated transition temperature $T_{\rm CDW}$ as a function of n for a range of fillings near $n = 1$ (SI Sec. E [21]); note that a fully insulating CDW is present only at the commensurate filling $n = 1$ (green vertical line in Fig. 1c). Next, we address the fate of this insulating CDW when doped with electrons or holes away from $n = 1$.

Furthermore, we analyze D_s at low temperature, $T = 0.008$, as a function of particle density (SI Sec. E [21]). We identify BKT transitions towards superconducting order and find the critical carrier densities $n_c = 0.923 \pm 0.006$ and $n_c = 1.062 \pm 0.008$ for hole and electron doping, respectively. Fig. 1(c) summarizes n_c for different temperatures. T_c vanishes for $n = 1$ and increases monotonically with $\delta n = |n - 1|$, suggesting that superconductivity arises due to excess ("doped") electrons or holes relative to the ordered CDW insulator. Importantly, along with superconductivity, the CDW remains long-range ordered. Thus the resulting phase is a supersolid, with a finite superconducting phase stiffness and a spontaneously broken lattice translational symme-

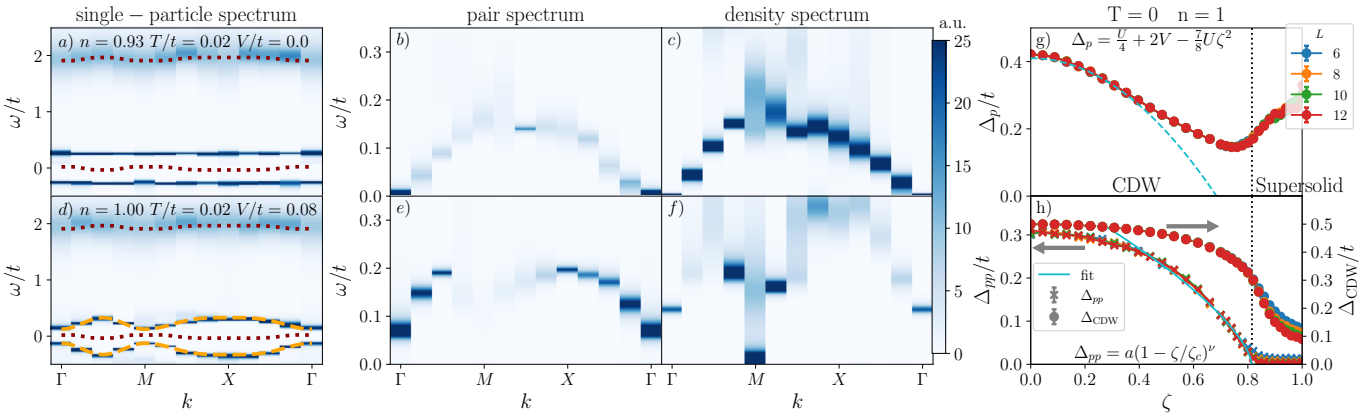

FIG. 3. Excitation spectra in the superconducting phase (a-c), in the CDW phase (d-f) at $T/t = 0.02$ [$\zeta = 0.75$], and excitation energies relative to the ground state (g-h): (a) and (d) show electronic spectra featuring the flat and interaction-induced dispersive bands (non-interacting bands in maroon). (b) and (e) show s-wave pair spectra. (c) and (f) show density spectra. (g) and (h) display the single- and two-particle excitation energies, respectively, of the ground state at quarter filling with $U = 1$ and $V = 0.08$. The turquoise fits depict the expectations from the density-assisted hopping (g) and 3D-XY universality (h).

try. The lightly doped system can effectively be described in terms of a dilute liquid of interacting bosons with a superconducting $T_c \propto \delta n$, up to additional logarithmic corrections [28–30].

We also examine the single and two-particle spectrum in the different phases [21]. We compute $A(\mathbf{k},\omega) = -\mathrm{Im}\, G(\mathbf{k},\omega)/\pi$ from the imaginary time Green's function, $G(\mathbf{k},\tau) = \sum_{l,s} \langle c_{\mathbf{k},l,s}(\tau) c^\dagger_{\mathbf{k},l,s}(0)\rangle$, and the pairing and density spectra via the maximum entropy method [31]. For $V = 0$, the resulting single and two-particle spectra are summarized in Figs. 3(a)-(c). The single electron spectrum exhibits two nearly flat bands at $\omega \approx \pm 0.25t$, that are well separated from a broader band at $\omega \approx 2t (= \Delta_{\rm gap})$. The latter is clearly the higher energy flat band associated with H_0. The bands at $\omega \approx \pm 0.25t$ originate from the low-energy flat band of H_0, that splits due to the Hubbard interaction; specifically, the splitting energy is approximately $\Delta_{S^z} = U/4$, the gap associated with the $\zeta = 0$ limit. The spectrum of pairing and density excitations show linearly dispersing, Goldstone-like modes near the $\Gamma-$point. These modes can be understood as arising from the approximate SU(2) symmetry of the attractive Hubbard interaction projected to the flat band [32].

For $V = 0.08$, the single and two-particle spectra are summarized in Figs. 3(d)-(f). The high-energy band at $\omega \approx 2t (= \Delta_{\rm gap})$ in Fig. 3(d) is nearly identical to the previous case. However, the low-energy bands are significantly more dispersive than in Fig. 3(a) due to the density-assisted hopping terms (Fig. 1) of the projected Hamiltonian. Note that adding a single electron to the background of the CDW, on the one hand, costs an energy $\bar{\Delta}$ due to breaking a pair and creating a point defect in the CDW; this accounts for the finite energy offset and, in the small ζ limit, this energy is $\bar{\Delta} = \frac{U_{\rm eff}}{2} - 4\Delta^2_{\rm CDW} J_z$ [21]. On the other hand, the electron can delocalize and gain kinetic energy due to the density-assisted hopping where the effective width of the shifted band scales as $U\zeta^2\Delta_{\rm CDW}$ with $\Delta_{\rm CDW} \equiv \langle e^{i\mathbf{r}\mathbf{q}_{\rm CDW}} \hat{\eta}^z_{\mathbf{r}}\rangle$ and $\mathbf{q}_{\rm CDW} = (\pi,\pi)$. The dispersion relation directly follows from the second term of Eq. (3) and is depicted as dashed orange lines in Fig. 3(d).

The two-particle spectra show that the linearly dispersing Goldstone mode near the $\Gamma-$point is gapped for $n = 1$ and $V = 0.08$, while the density spectrum (Fig. 3f) exhibits a clear softening near the CDW ordering wavevector. Increasing ζ while keeping all other parameters fixed, we have extracted the single-particle and two-particle gaps, Δ_p and Δ_{pp}, at $T = 0$ near the $\Gamma-$point (Figs. 3g-h, respectively). For $\zeta < 0.7$, Δ_p decreases with increasing ζ, in agreement with the expectation $\Delta_p = \frac{U}{4} + 2V - \frac{7}{8}U\zeta^2$ [21]. Δ_p assumes its minimal value at $\zeta \approx 0.75$. Similarly, Δ_{pp} is largest for $\zeta = 0$ and decreases with increasing ζ (Fig. 3 h), vanishing for $\zeta > 0.815$. It is important to note that the onset of superconductivity at $\zeta_c = 0.815$, as inferred from the behavior of $\xi_{\rm SC}/L$ (Fig. 1d), is accompanied by a finite $\Delta_{\rm CDW}$; the transition from CDW to supersolid order belongs in the $(2+1)$-dimensional XY universality class. In the pseudospin notation introduced in Eq. 3, the supersolid is represented by a canted antiferromagnet, where the in-plane (XY) ferromagnetic components represent the SC while the out-of-plane antiferromagnetic component represents the CDW.

Discussion.- Our work highlights phase competition in flat bands with vanishing Berry curvature but non-trivial Fubini-Study metric. By construction, these systems are strongly correlated; in addition, due to the band geometry, quantum fluctuations are important even in the perfectly flat band limit. As a result, the phase diagram can

be difficult to predict a priori, without controlled calculations.

We have demonstrated this by a sign problem-free, explicitly solvable model with a tunable quantum metric. The model exhibits a cascade of quantum phases. The interactions within the flat band lead to the formation of a CDW phase, whose electronic excitations acquire a nontrivial dispersion due to the band geometry. Increasing this dispersion by tuning the quantum metric ultimately leads to a further instability towards a supersolid phase.

We expect such cascades of different ordering tendencies to arise also in realistic flat-band systems, such as those that occur in two-dimensional van der Waals materials. Additionally, there is a promising prospect to engineer and directly simulate some elements of the models considered here in future cold-atoms based experiments. Recent experiments using ultracold bosonic atoms have identified supersolids in one [33–37] and two dimensions [38, 39]. Realizing supersolids in models of fermionic ultracold atoms [40–42] remains an interesting open challenge, but can potentially be realized using the setups proposed here.

Furthermore, our work unambiguously demonstrates that any proposed lower bound on the superfluid stiffness in terms of single-properties of the flat band, such as the quantum geometry, are strictly inapplicable beyond BCS mean-field theory. In the presence of a large on-site attraction and weak nearest-neighbor repulsion, where application of the mean-field approximation will lead one to conclude a superconducting ground state with a nonzero superfluid stiffness, our exact computations show that the stiffness can be made arbitrarily small and even vanish, violating any putative bound.

Acknowledgements.- The authors thank Ankur Das, Tobias Holder, and Steven Kivelson for stimulating discussions. DC is supported by faculty startup funds at Cornell University. EB and JH were supported by the European Research Council (ERC) under grant HQMAT (grant no. 817799), the US-Israel Binational Science Foundation (BSF), and a Research grant from Irving and Cherna Moskowitz. This work used the Extreme Science and Engineering Discovery Environment (XSEDE), which is supported by National Science Foundation grant number ACI-1548562 [43]. The authors gratefully acknowledge the generous computing time on Expanse at the San Diego Supercomputer Center through allocation TG-PHY210006. We also thank Cyrus Umrigar for sharing his computational resources (TG-PHY170037) at the early stages of this work. The auxiliary field QMC simulations were carried out using the ALF package available at https://alf.physik.uni-wuerzburg.de.

[1] E. Y. Andrei, D. K. Efetov, P. Jarillo-Herrero, A. H. MacDonald, K. F. Mak, T. Senthil, E. Tutuc, A. Yazdani, and A. F. Young, The marvels of moiré materials, Nat. Rev. Mater. **6**, 201 (2021).

[2] P. Törmä, S. Peotta, and B. A. Bernevig, Superconductivity, superfluidity and quantum geometry in twisted multilayer systems, Nat. Rev. Phys. **4**, 528 (2022), arXiv:2111.00807.

[3] V. Shaginyan and V. Khodel, Superfluidity in system with fermion condensate, JETP Lett **51** (1990).

[4] T. T. Heikkilä, N. B. Kopnin, and G. E. Volovik, Flat bands in topological media, Sov. J. Exp. Theor. Phys. Lett. **94**, 233 (2011), arXiv:1012.0905 [cond-mat.str-el].

[5] G. E. Volovik, Flat band in topological matter, J. Supercond. Nov. Magn. **26**, 2887 (2013).

[6] N. Marzari, A. A. Mostofi, J. R. Yates, I. Souza, and D. Vanderbilt, Maximally localized wannier functions: Theory and applications, Rev. Mod. Phys. **84**, 1419 (2012).

[7] S. Peotta and P. Törmä, Superfluidity in topologically nontrivial flat bands, Nat. Commun. **6**, 8944 (2015).

[8] R. Blankenbecler, D. J. Scalapino, and R. L. Sugar, Monte carlo calculations of coupled boson-fermion systems. i, Phys. Rev. D **24**, 2278 (1981).

[9] J. S. Hofmann, E. Berg, and D. Chowdhury, Superconductivity, pseudogap, and phase separation in topological flat bands, Phys. Rev. B **102**, 201112 (2020).

[10] V. Peri, Z.-D. Song, B. A. Bernevig, and S. D. Huber, Fragile topology and flat-band superconductivity in the strong-coupling regime, Phys. Rev. Lett. **126**, 027002 (2021).

[11] X. Zhang, K. Sun, H. Li, G. Pan, and Z. Y. Meng, Superconductivity and bosonic fluid emerging from moiré flat bands, Phys. Rev. B **106**, 184517 (2022), arXiv:2111.10018v3.

[12] J. Herzog-Arbeitman, V. Peri, F. Schindler, S. D. Huber, and B. A. Bernevig, Superfluid Weight Bounds from Symmetry and Quantum Geometry in Flat Bands, Phys. Rev. Lett. **128**, 087002 (2022), arXiv:2110.14663.

[13] M. Tovmasyan, S. Peotta, P. Törmä, and S. D. Huber, Effective theory and emergent SU(2) symmetry in the flat bands of attractive hubbard models, Phys. Rev. B **94**, 245149 (2016).

[14] F. Xie, Z. Song, B. Lian, and B. A. Bernevig, Topology-bounded superfluid weight in twisted bilayer graphene, Phys. Rev. Lett. **124**, 167002 (2020).

[15] X. Hu, T. Hyart, D. I. Pikulin, and E. Rossi, Geometric and conventional contribution to the superfluid weight in twisted bilayer graphene, Phys. Rev. Lett. **123**, 237002 (2019).

[16] A. Julku, T. J. Peltonen, L. Liang, T. T. Heikkilä, and P. Törmä, Superfluid weight and berezinskii-kosterlitz-thouless transition temperature of twisted bilayer graphene, Phys. Rev. B **101**, 060505 (2020).

[17] T. Hazra, N. Verma, and M. Randeria, Bounds on the superconducting transition temperature: Applications to twisted bilayer graphene and cold atoms, Phys. Rev. X **9**, 031049 (2019).

[18] N. Verma, T. Hazra, and M. Randeria, Optical spectral weight, phase stiffness, and T_c bounds for trivial and topological flat band superconductors, Proc. Natl. Acad. Sci. **118**, e2106744118 (2021).

[19] D. Mao and D. Chowdhury, Diamagnetic response and phase stiffness for interacting isolated narrow bands, Proc. Natl. Acad. Sci. **120**, e2217816120 (2023).

[20] J. S. Hofmann, D. Chowdhury, S. A. Kivelson, and E. Berg, Heuristic bounds on superconductivity and how to exceed them, npj Quantum Mater. **7**, 83 (2022).

[21] See supplementary information for additional details on computations for the wannier wave function, the quantum geometric tensor and its connection with the orbital embedding, the projected hamiltonian, the correlation length for cdw, and the particle-excitation gaps.

[22] S. H. Simon and M. S. Rudner, Contrasting lattice geometry dependent versus independent quantities: Ramifications for Berry curvature, energy gaps, and dynamics, Phys. Rev. B **102**, 165148 (2020).

[23] M. Bercx, F. Goth, J. S. Hofmann, and F. Assaad, The alf (algorithms for lattice fermions) project release 1.0. documentation for the auxiliary field quantum monte carlo code, SciPost Phys. **3**, 013 (2017), arXiv:1704.00131 [cond-mat.str-el].

[24] F. Assaad, M. Bercx, F. Goth, A. Götz, J. Hofmann, E. Huffman, Z. Liu, F. Parisen Toldin, J. Portela, and J. Schwab, The ALF (Algorithms for Lattice Fermions) project release 2.0. Documentation for the auxiliary-field quantum Monte Carlo code, SciPost Phys. Codebases , 1 (2022), arXiv:2012.11914.

[25] D. R. Nelson and J. M. Kosterlitz, Universal jump in the superfluid density of two-dimensional superfluids, Phys. Rev. Lett. **39**, 1201 (1977).

[26] D. J. Scalapino, S. R. White, and S. Zhang, Insulator, metal, or superconductor: The criteria, Phys. Rev. B **47**, 7995 (1993).

[27] F. Parisen Toldin, M. Hohenadler, F. F. Assaad, and I. F. Herbut, Fermionic quantum criticality in honeycomb and π-flux hubbard models: Finite-size scaling of renormalization-group-invariant observables from quantum monte carlo, Phys. Rev. B **91**, 165108 (2015).

[28] V. N. Popov, On the theory of the superfluidity of two- and one-dimensional bose systems, Theor. Math. Phys. **11**, 565 (1972).

[29] Y. Kagan, B. Svistunov, and G. Shlyapnikov, Influence on inelastic processes of the phase transition in a weakly collisional two-dimensional bose gas, Sov. Phys. JETP **66**, 314 (1987).

[30] D. S. Fisher and P. C. Hohenberg, Dilute bose gas in two dimensions, Phys. Rev. B **37**, 4936 (1988).

[31] K. S. D. Beach, Identifying the maximum entropy method as a special limit of stochastic analytic continuation, arXiv e-prints , cond-mat/0403055 (2004), arXiv:cond-mat/0403055 [cond-mat.str-el].

[32] A. Julku, S. Peotta, T. I. Vanhala, D.-H. Kim, and P. Törmä, Geometric origin of superfluidity in the lieb-lattice flat band, Phys. Rev. Lett. **117**, 045303 (2016).

[33] J.-R. Li, J. Lee, W. Huang, S. Burchesky, B. Shteynas, F. Ç. Top, A. O. Jamison, and W. Ketterle, A stripe phase with supersolid properties in spin–orbit-coupled Bose–Einstein condensates, Nature **543**, 91 (2017).

[34] J. Léonard, A. Morales, P. Zupancic, T. Esslinger, and T. Donner, Supersolid formation in a quantum gas breaking a continuous translational symmetry, Nature **543**, 87 (2017), arXiv:1609.09053.

[35] L. Tanzi, S. M. Roccuzzo, E. Lucioni, F. Famà, A. Fioretti, C. Gabbanini, G. Modugno, A. Recati, and S. Stringari, Supersolid symmetry breaking from compressional oscillations in a dipolar quantum gas, Nature **574**, 382 (2019), arXiv:1906.02791.

[36] M. Guo, F. Böttcher, J. Hertkorn, J. N. Schmidt, M. Wenzel, H. P. Büchler, T. Langen, and T. Pfau, The low-energy Goldstone mode in a trapped dipolar supersolid, Nature **574**, 386 (2019), arXiv:1906.04633.

[37] G. Natale, R. M. W. van Bijnen, A. Patscheider, D. Petter, M. J. Mark, L. Chomaz, and F. Ferlaino, Excitation Spectrum of a Trapped Dipolar Supersolid and Its Experimental Evidence, Phys. Rev. Lett. **123**, 050402 (2019), arXiv:1907.01986.

[38] M. A. Norcia, C. Politi, L. Klaus, E. Poli, M. Sohmen, M. J. Mark, R. N. Bisset, L. Santos, and F. Ferlaino, Two-dimensional supersolidity in a dipolar quantum gas, Nature **596**, 357 (2021), arXiv:2102.05555.

[39] G. Biagioni, N. Antolini, A. Alaña, M. Modugno, A. Fioretti, C. Gabbanini, L. Tanzi, and G. Modugno, Dimensional Crossover in the Superfluid-Supersolid Quantum Phase Transition, Phys. Rev. X **12**, 021019 (2022), arXiv:2111.14541.

[40] I. Bloch and M. Greiner, The superfluid-to-Mott insulator transition and the birth of experimental quantum simulation, Nat. Rev. Phys. **4**, 739 (2022).

[41] T. Esslinger, Fermi-Hubbard Physics with Atoms in an Optical Lattice, Annu. Rev. Condens. Matter Phys. **1**, 129 (2010).

[42] C. J. Vale and M. Zwierlein, Spectroscopic probes of quantum gases, Nature Physics **17**, 1305 (2021).

[43] J. Towns, T. Cockerill, M. Dahan, I. Foster, K. Gaither, A. Grimshaw, V. Hazlewood, S. Lathrop, D. Lifka, G. D. Peterson, R. Roskies, J. R. Scott, and N. Wilkins-Diehr, XSEDE: Accelerating Scientific Discovery, Comput. Sci. Eng. **16**, 62 (2014).